Published in final edited form as:
Cardiovasc Eng Technol. 2010 March ; 1(1): . doi:10.1007/s13239-010-0004-8.

Supraceliac and Infrarenal Aortic Flow in Patients with Abdominal Aortic Aneurysms: Mean Flows, Waveforms, and Allometric Scaling Relationships

Andrea S. Les[1], **Janice J. Yeung**[2], **Geoffrey M. Schultz**[2], **Robert J. Herfkens**[3], **Ronald L. Dalman**[2], and **Charles A. Taylor**[1,4]

[1]Department of Bioengineering, Stanford University, Stanford, CA, USA

[2]Division of Vascular Surgery, Stanford University, Stanford, CA, USA

[3]Department of Radiology, Stanford University, Stanford, CA, USA

[4]James H. Clark Center, Room E350B, 318 Campus Drive, Stanford, CA 94305-5431, USA

Abstract

Purpose—Hemodynamic forces are thought to play a critical role in abdominal aortic aneurysm (AAA) growth. *In silico* and *in vitro* simulations can be used to study these forces, but require accurate aortic geometries and boundary conditions. Many AAA simulations use patient-specific geometries, but utilize inlet boundary conditions taken from a single, unrelated, healthy young adult.

Methods—In this study, we imaged 43 AAA patients using a 1.5 T MR scanner. A 24-frame cardiac-gated one-component phase-contrast magnetic resonance imaging sequence was used to measure volumetric flow at the supraceliac (SC) and infrarenal (IR) aorta, where flow information is typically needed for simulation. For the first 36 patients, individual waveforms were interpolated to a 12-mode Fourier curve, peak-aligned, and averaged. Allometric scaling equations were derived from log–log plots of mean SC and IR flow vs. body mass, height, body surface area (BSA), and fat-free body mass. The data from the last seven patients were used to validate our model.

Results—Both the SC and IR averaged waveforms had the biphasic shapes characteristic of older adults, and mean SC and IR flows over the cardiac cycle were 51.2 ± 10.3 and 17.5 ± 5.44 mL/s, respectively. Linear regression of the log–log plots revealed that BSA was most strongly predictive of mean SC (R^2 = 0.29) and IR flow (R^2 = 0.19), with the highest combined R^2. When averaged, the measured and predicted waveforms for the last seven patients agreed well.

Conclusions—We present a method to estimate SC and IR mean flows and waveforms for AAA simulation.

Keywords

Phase-contrast magnetic resonance imaging (PC-MRI); Weight; Body surface area (BSA); Linear regression; Biphasic waveform

Address correspondence to Charles A. Taylor, James H. Clark, Center, Room E350B, 318 Campus Drive, Stanford, CA 94305-5431, USA. taylorca@stanford.edu.

INTRODUCTION

Hemodynamic conditions are thought to play a critical role in abdominal aortic aneurysm (AAA) formation, growth, and rupture, and may contribute to migration and failure of endovascular aortic grafts.[10] Simulation of blood flow enables the study of such hemodynamic conditions but requires both accurate geometries *and* boundary conditions, the latter usually in the form of volumetric flow and pressure data at specific locations. Ideally, the inlet boundary condition— typically volumetric flow—and AAA geometry would be acquired from the same patient. While this truly patient-specific method has been successfully employed by some studies,[19,26] technical limitations to data acquisition make AAA geometric information more abundant than flow data.

Hundreds of computed tomography (CT) and magnetic resonance (MR) imaging studies of AAA geometry are performed daily to monitor AAA growth, plan for AAA repair, and monitor endovascular graft placement, making detailed, 3D anatomic data about AAAs widely available. Unfortunately, volumetric flow data are more scarce. Flows can be measured invasively with a flow catheter, but this poses a nontrivial risk to the patient. Noninvasive imaging modalities used in AAA surveillance, such as CT, ultrasound, and magnetic resonance imaging (MRI), either provide limited flow information or are rarely used to measure flow in a clinical setting. CT, for example, does not measure flow. Ultrasound, on the other hand, is a widely available, inexpensive, and low-risk method often used to monitor long-term AAA growth, but can provide only limited volumetric flow information. Pulsed-wave ultrasound, for example, typically quantifies only a single peak, centerline, or average velocity waveform at a given vessel cross section; thus, volumetric flow derived from pulsed-wave ultrasound data must be inferred from a theoretical velocity profile and averaged diameter measurements. [15] Volumetric flow can also be measured from color Doppler images, but this technique can be plagued by underestimation due to angle of approach.[15] More importantly, though, ultrasound is rarely used to measure velocities or flows in AAAs clinically, as this information is not used in AAA surveillance. Some MR imaging techniques, such as 2D phase-contrast magnetic resonance imaging (PC-MRI), are excellent for acquiring flow data: flow velocities in a plane of arbitrary orientation are measured and integrated over the vessel lumen, yielding volumetric flow.[19] However, similar to ultrasound, MRI scan protocols for AAA surveillance rarely include acquisition of PC-MRI data, due to a lack of clinical application for flow data. Therefore, as a result of significant logistic and theoretical limitations to *de novo* acquisition of same-patient anatomic and volumetric flow data, many published AAA blood flow simulations use highly resolved patient-specific geometries that were obtained clinically, but utilize literature-derived volumetric flows for the inlet boundary condition, which may be derived from a completely unrelated healthy person of dissimilar body size, age, gender, and medical history.

Fraser *et al*.[11] pointed out that the majority of AAA computational hemodynamic simulations rely on waveform data from one of two papers: Mills *et al*. used an invasive catheter to measure velocity and pressure waveforms in the major arteries of 23 patients, but presented pressure and velocity waveform results for an individual patient only,[20] while Olufsen *et al*. used PC-MRI to measure volumetric flow in a single, young, healthy male.[22] The work of Fraser *et al*. marks an important first step in compiling inlet flow data in actual AAA patients. In this study, ultrasound was used to measure centerline velocity waveforms in 31 AAA patients (10 of whom were later excluded) at the infrarenal (IR) level. Then, a volumetric flow waveform was calculated assuming a Womersley velocity profile and using averaged diameter information from eight AAA patients. While using the volumetric flow waveforms presented in Fraser *et al*. for an inlet boundary condition for AAA simulation is preferable to using velocity or flow data measured in a single, healthy, young person, the

data in Fraser *et al*. does not represent an average of volumetric flows measured directly in AAA patients. Cheng *et al*. used PC-MRI to directly measure supraceliac (SC) and IR aortic flow in eight older, nonaneurysmal subjects; however, the waveforms published are for a single, representative patient, rather than an average of all waveforms.[3]

An ideal compilation of AAA flow data would exhibit a variety of features. First, since volumetric flow, not velocity, is generally needed for hemodynamic simulation, the ideal AAA flow data would consist of direct measurements of volumetric flows, rather than extrapolation of volumetric flow from a single centerline velocity waveform and an assumed velocity profile. Second, flow information sufficiently proximal to the AAA, and from more than one proximal location, is desired. Ideally, a AAA computational model would begin at the aortic valve, and flow would be prescribed as it is exiting the heart, such that the flow has sufficient time and space to develop aperiodicity and swirling down the length of the aorta before it enters an AAA. However, it is not common to image the entire torso for AAA surveillance. InMRI AAA scans, for example, both the size of the receiver coil and imaging time constraints mean that only mid-to-lower abdomen data are acquired. Thus, computational models should begin at the top of the imaging data; this typically corresponds to the SC location. As with any computational simulation of blood flow where patient-specific flow information is not available, researchers will have to make some assumption about the velocity profile at this location. Furthermore, we argue that computational studies of hemodynamics in AAA that use models that begin at the IR level are not ideal. In these studies, an IR volumetric flow waveform is typically mapped to the inlet of a AAA geometric model using an axisymmetric and periodic velocity profile, such as the Womersley profile.[19,26,29] However, it is unlikely that IR flow is actually axisymmetric in a AAA patient, as the nearby renal arteries (which are not themselves symmetrically placed along the aorta) pull flow laterally and the superior mesenteric artery and celiac artery pull flow anteriorly. In addition, if one wishes to assess whether turbulence is present, prescribing periodic flow at the IR level may lead to misleading results. Our previous work, which utilized computational models that begin at the SC level, shows that turbulence is indeed present within AAAs, and that this turbulence sometimes extends to the IR location.[19] Because AAAs may begin just distal to or even overlap the renal artery ostia, prescribing a periodic flow at the IR level may lead to the appearance of less turbulence in the aneurysm than is actually present. Furthermore, performing simulations over several cardiac cycles with models that begin at the SC level allows IR flow to be nonperiodic, essential for the study of aneurysmal turbulence.

Lastly, aneurysmal disease affects people of all shapes and sizes, and aortic flow may differ widely from person to person depending on body size. Allometric scaling laws, which describe the relationship between structural or functional parameters and body size, offer one way to account for widely varying body size. Allometric scaling laws are usually nonlinear and are of the form: $Y = Y_0 M^b$, where Y is the parameter of interest (such as mean flow), Y_0 is a normalization constant, M is a measure of body size (such as body mass or height), and b is the scaling exponent. Previous studies have used allometric scaling relationships to theoretically and experimentally define the relationship between mean flow and body mass across species, [9,13,25,28] while other investigators have related cardiac output (CO) to body mass, body surface area (BSA), and height in children and adults.[6] For example, this latter study found an allometric scaling relationship between CO and body mass in normal-weight adults of the form: CO in mL/min = 235 (weight in kg)$^{0.71}$.[6] By this relationship, we can estimate that a 130-pound (59.0-kg) person would have a CO of 4248 mL/min or 70.8 mL/s, whereas a 210-pound (95.3-kg) person would have a CO of 5971 mL/min or 99.5 mL/s. Thus, while the 210-pound person is 61.5% heavier than the 130 lb person, the 210-pound person has only a 40.6% greater CO. Clearly, using a flow waveform measured in a 130-pound patient for a blood flow simulation in a 210-pound patient would

not be ideal. This severe underestimation of mean flow, as well as the concomitant inaccuracies in minimum and maximum flows, could lead to inaccurate pressures, velocities, flow splits, shear stresses, oscillatory shear indices, and turbulence.

In the absence of patient-specific flow information, it would be desirable for an AAA simulation to pre-scribe an inlet flow that is (1) based on a waveform derived from primary imaging data acquired in a large number of AAA patients and (2) proportional to the patient's body size. In this paper, we present SC and IR volumetric flow waveforms measured via PC-MRI from 43 AAA patients who were imaged as part of a larger NIH-sponsored study examining the effects of exercise on AAA progression.[5] To our knowledge, this is the largest collection of PC-MRI data in an AAA population. We used the first 36 patients compute a model for scaling SC and IR flows for different body sizes. Specifically, we report mean SC and IR flows, peak-aligned and averaged SC and IR flow waveforms, and allometric scaling relationships for mean SC and IR flows vs. body mass, height, BSA, and fat-free body mass (FFBM). We used the remaining seven patients (patients 37 through 43) to validate our model. We hereafter refer to the first 36 patients as our "model cohort" and to the last seven patients as our "validation cohort." Thus, this work describes the volumetric flow features occurring superior to the AAA at the SC and IR locations and provides a highly generalizable method to derive more accurate boundary conditions for AAA hemodynamic simulation in humans. We hope that this, in turn, will lead to a deeper understanding of AAA pathophysiology, as well as prove useful in the design of aortic stent grafts used to repair AAAs, which are often affixed at the IR and SC locations.

METHODS

Imaging

Between April 2007 and June 2009, we imaged 45 male patients and one female patient with a history of small AAAs (diameter <5 cm) who were enrolled in an NIH-sponsored study examining whether prescribed exercise may slow the growth of AAA.[5] Imaging studies were conducted under a protocol approved by the local institutional review board, informed consent was obtained from all subjects, and all patients were screened for contraindications to MRI and gadolinium usage.[27] Patients with an estimated renal glomerular filtration rate (eGFR) below 30 mL/min/1.73 m^2 were not imaged,[27] and all patients were asked to fast for 2 h prior to the scan to minimize intestinal motion during image acquisition. Patients were imaged in the supine position using a 1.5 T GE Signa MR scanner (GE Medical Systems, Milwaukee WI) and an 8-channel cardiac coil. A 3D gadolinium-enhanced magnetic resonance angiography (MRA) sequence was used to image the lumen of the aneurysmal aorta (Fig. 1). Next, an electrocardiograph-gated (ECG-gated), respiratory-compensated, one-component (through-plane) PC-MRI sequence was prescribed from the coronal MRA and an oblique localizer scan, such that the PC-MRI sequence was positioned perpendicular to the long axis of the aorta. The SC slice was prescribed a few centimeter above the celiac artery, and the IR slice was prescribed a few centimeter below the lowest renal artery, so that any breathing motion would not bring these arteries into the PC-MRI slice.[7] If accessory renal arteries were noted on the MRA immediately after acquisition, the IR slice was prescribed below the lowest renal artery. For three male patients, accessory renal arteries were noted below the IR imaging plane during post-processing; their data were excluded from further analysis, leaving 42 male and 1 female AAA patients. Data from the first 36 patients (the "model cohort", patients 1 through 36, imaged between April 2007 and March 2009) were used in this study to compute and derive mean SC and IR flows, peak-aligned and averaged waveforms, and allometric scaling equations. Results from the last seven patients (the "validation cohort", patients 37 through 43, imaged between April and June 2009) were used to validate the model.

Imaging parameters for the gradient-recalled echo PC-MRI sequence included: a 256 × 192 acquisition matrix (reconstructed to 256 × 256), 5-mm slice thickness, 11.9–12.7 ms TR, 4.5–5.4 ms TE, 20° flip angle, 24–34 cm square FOV, two signal averages, and respiratory compensation. A velocity encoding gradient of 150 cm/s through-plane was used, and the data were interpolated to 24 time frames. The temporal resolution was two times the TR, or 23.8–25.4 ms. Brachial systolic and diastolic blood pressure, also useful for simulation, were recorded immediately after the scan using an automated pressure cuff (Omron Healthcare Inc., Bannockburn, IL, USA).

For each patient at each location, the aortic lumen was segmented using a thresholding or level-set technique at each of the 24 time frames in the PC-MRI magnitude images. Next, the average velocity within each segmentation was computed and multiplied by the corresponding segmentation area to generate a volumetric flow for that time frame. These 24 volumetric flows then underwent baseline correction using a linear correction algorithm to eliminate distortion from gradient inhomogeneities arising from eddy currents, and were then assembled into a volumetric flow waveform (Fig. 2). Flows then underwent peak alignment by first fitting a 12-mode Fourier spline (defined at 1000 points) to each waveform, aligning each curve at its maximum, and down-sampling back to 24 points (Fig. 3). Mean SC and IR flows, as well as average SC and IR waveforms were then calculated from the newly aligned individual waveforms (Fig. 4).

Allometric Scaling Metrics

Body size metrics used for the allometric scaling equations of the form $Y = Y_0 M^b$ were recorded or calculated as follows. Patient weight (body mass) and height were recorded at study intake. BSA was calculated as[21]:

$$BSA = \left(\frac{HM}{36}\right)^{\frac{1}{2}}, \quad (1)$$

where H is height (m) and M is mass (kg). *FFBM* was calculated from Garrow and Webster as[2,12]:

$$FFBM = M(1-C) + (DH^2), \quad (2)$$

where M is body mass in kg, H is height in m, and C is 0.715 and 0.713, and D is 12.1 and 9.74 for men and women, respectively. Lastly, we plotted the mean IR and SC flows against body mass, height, BSA, and FFBM on a log–log scale and used linear regression to determine the allometric coefficients:

$$Y = Y_0 M^b \quad (3)$$

$$\log(Y) = \log(Y_0 M^b) \quad (4)$$

$$\log(Y) = \log Y_0 + b\log(M). \quad (5)$$

Equation (3) is the initial allometric scaling relationship, and Eq. (5) is the linear relationship used for the log–log plots. Note that ($\log Y_0$) is the *y*-intercept in the linear equation.

Model Validation

Data from the validation cohort (patients 37 through 43) were not used to compute the mean flows, peak-aligned and averaged waveforms, or the allometric scaling equations, and could thus be used to validate our model. For each of these patients, we predicted mean SC and IR flows based on the patient's BSA. We then compared this prediction to the measured mean SC and IR flows. We also predicted SC and IR waveforms for each patient by scaling the average waveforms presented in Fig. 4 by each patient's predicted mean flow. For example, if a patient's predicted mean IR flow was 14.1 mL/s based on their BSA, the average IR waveform presented in Fig. 4 would be scaled by a factor of $\frac{14.1\ \mathrm{mL/s}}{17.5\ \mathrm{mL/s}}=0.806$, where 17.5 mL/s is the mean IR flow computed from the model cohort. We then compared the predicted SC and IR waveforms (averaged over seven patients) to the measured SC and IR waveforms (peak-aligned and averaged over seven patients). The predicted waveforms did not require peak-alignment because they were all scaled versions of the same waveform.

RESULTS

Patient Cohort

The gender distribution, mean age, average SC flow, average IR flow, IR/SC flow ratio, heart rate at SC acquisition, heart rate at IR acquisition, body mass, height, BSA, FFBM, body mass index (BMI), systolic and diastolic brachial blood pressures, and estimated glomerular filtration rate (eGFR) for both the model (n = 36) and validation (n = 7) cohorts are shown in Table 1. For the model cohort, the heart rates recorded at the beginning of the SC and IR PC-MRI measurements were very similar (63.3 ± 11.0 beats per minute (bpm) for SC and 62.9 ± 10.5 bpm for IR). The mean BMI (27.4 ± 2.74 kg/m^2) indicates that our patient cohort was overweight but not obese. It is important to note that the dimensions of our MR scanner excluded some obese and all very obese AAA patients from our study: the largest BMI among our patients was 33.2, indicating mild obesity. The systolic and diastolic blood pressures indicate that our patient population was, on average, borderline hypertensive, a common characteristic of AAA patients.[18] The mean eGFR, a metric necessary to determine if it is safe to administer gadolinium,[27] indicated borderline-normal renal function. There was no statistical difference (p>0.05) between the model and validation cohort for any of the values reported in Table 1.

Waveform Shape

Peak-aligned, averaged SC and IR volumetric waveforms (Fig. 4) show a biphasic morphology at both locations, with fairly constant flow during diastole. Averaged SC flow remained positive throughout the cardiac cycle, though it approached zero at end-systole. The IR flow waveform displayed significant reverse flow at end-systole, with fairly constant zero or near-zero flow during diastole.

Allometric Scaling Relationships

The log–log plots of mean SC and IR flow vs. body mass, height, BSA, and FFBM, and their associated linear regression equations and R^2 values are shown in Fig. 5. Recall from Eq. (5) that in the linear equations presented in Fig. 5, the coefficients for M and the y-axis intercepts are exactly the exponent, b, and the $\log_{10}$ of the normalization constant Y_0, respectively. Thus, while the scaling exponent, b, remains the same, the normalization constant, Y_0, can be recovered by taking $10^{y\text{-intercept}}$. All eight allometric scaling equations, their R^2-values, and the p-values for b and $\log(Y_0)$ are summarized in Table 2. The p-values for the scaling exponent, b, indicate statistical significance in each allometric equation, with the exception of mean IR flow vs. height. Mean SC and IR flow vs. BSA had the highest combined R^2-values (0.29 for mean SC flow and 0.19 for mean IR flow).

Model Validation

A comparison between predicted and measured mean SC and IR flows for our validation cohort (patients 37 through 43) can be seen in Table 3. The mean percent difference between the predicted and measured flow was −5.10 ± 18.9% for SC and −4.47 ± 25.3% for IR. The absolute value of the percent difference between predicted and measured flows differed by an average of 15.2 ± 10.9% for SC and 18.0 ± 16.9% for IR. A comparison between predicted and measured SC and IR flow waveforms (averaged over the seven patients) can be seen in Fig. 6.

DISCUSSION

We have measured aortic volumetric flow in 43 patients with small AAAs at the SC and IR levels using PC-MRI and MRA imaging techniques. In this study, we provide mean SC and IR flows, peak-aligned and averaged waveforms, and allometric scaling relationships derived from 36 AAA patients, and then use seven additional AAA patients to validate our model. To the best of our knowledge, this is the largest collection of PC-MRI flows measured in a AAA population, and the first presentation of allometric scaling relationships for mean SC and IR flows. We hope that these results will enable future hemodynamic simulation studies to compute and use more accurate SC and IR waveforms scaled to a particular patient's body size, as well as illuminate the flow conditions occurring superior to AAAs at the SC and IR location.

Comparison to Literature

To the best of our knowledge, the only published aortic flow data measured from PC-MRI in a population similar in age and gender to our cohort is from a previous study of aortic flow in older, healthy, nonaneurysmal adults.[3] Our patients differed from the earlier cohort in several key ways, including number of subjects (36 in our study vs. 8 in Cheng *et al*.), age (70.9 ± 6.73 in our study vs. 57.1 ± 3.4 years in Cheng *et al*.), weight (86.2 ± 9.53 kg in our study vs. 76.6 ± 15.0 kg in Cheng *et al*.), body position during imaging (supine in our study vs. upright in Cheng *et al*.), field strength of the magnet used in the studies (1.5 T in our study vs. 0.5 T in Cheng *et al*.), and the presence of vascular disease. The mean SC and IR flows (51.2 ± 10.3 mL/s or 3.07 ± 0.618 L/min for SC; 17.5 ± 5.44 mL/s or 1.05 ± 0.326 L/min for IR) calculated here were slightly greater than those reported in Cheng *et al*. (SC = 2.3 ± 0.4 L/min, IR = 0.9 ± 0.3 L/min).[3] However, our patients, at an average of 86.2 ± 9.53 kg, were significantly heavier than the patients reported by Cheng *et al*. (76.6 ± 15.0 kg), and thus higher mean SC and IR flows are to be expected. Indeed, plotting the mean SC and IR flows vs. body mass from the patients in Cheng *et al*. on our log–log plots (Fig. 5) showed good agreement with our trend lines. Moreover, our SC and IR waveforms agree with Cheng's single, representative SC and IR waveforms, in that all exhibited a biphasic shape, with fairly constant flow during diastole, SC flow approaching zero during end-systole and then remaining positive and relatively constant during diastole, and IR flow with significant flow reversal at end-systole and then constant zero or near-zero flow for the remainder of diastole. The simultaneous occurrence of very low positive SC flow and reverse IR flow observed in our peak-aligned, averaged waveform supports previous suggestions that the abdominal aorta may act as a capacitor,[14] with the reverse flow likely being delivered upstream to the renal arteries, which demand a comparatively high, positive flow during diastole.[1] It is important to note that the representative IR flow waveforms from *younger* patients (mean age 20–30 years) reported in an earlier publication by Cheng *et al*.[4] and Olufsen *et al*.[22] were triphasic in shape, with nonconstant diastolic flow, supporting the theory that aortic waveform morphology becomes biphasic in older patients due to age-related stiffening of the arteries and the concomitant loss of capacitance of the aorta and downstream vessels.

Our IR averaged waveform (Fig. 4) is significantly different than the ultrasound-derived IR volumetric flow waveform reported by Fraser *et al*.[11] Their mean IR flow value of 13.3 mL/s was lower than ours (17.5 ± 5.44 mL/s), and their reverse flow region accounted for approximately 1/3 of a cardiac cycle, much more than in our average IR waveform. In addition, their maximum and minimum flow values (max = ~150 mL/s; min = ~−60 mL/s) were higher and lower than our maximum and minimum flow values (max = 114 ± 28.0 mL/s; and min = −14.2 ± 12.7 mL/s). Aside from the lack of SC data in Fraser *et al*. (likely requiring that IR flow be mapped to the inflow face using an axisymmetric profile), these differences could significantly affect the results of computational simulations that use the Fraser waveform as an inlet boundary condition. For example, because reverse flow takes up a larger portion of the cardiac cycle in the Fraser *et al*. waveform, the calculated oscillatory shear index,[19,26] which measures the unidirectionality of shear stress, may be artificially elevated, incorrectly indicating that shear is more oscillatory than in actuality. Fraser *et al*. asserted that only ultrasound (not MRI) has sufficient temporal resolution to characterize the waveform. However, we note that one-component PC-MRI, which has a maximum temporal resolution of approximately 24 ms, has sufficient temporal resolution to capture the waveform shapes at the SC and IR levels. Furthermore, the Fraser study measured velocities over only a few cardiac cycles, whereas PC-MRI, by necessity, acquires data over nearly 400 heart beats. This minimizes the error due to irregular heartbeats caused by atrial fibrillation or ECG sensor or gating errors. Ultrasound is additionally limited by operator variation in obtaining a perfectly orthogonal vessel cross-sectional area, as well as uncertainty in determining which velocity profile to use when deriving volumetric flow from a single, centerline velocity measurement.[23]

Our scaling exponents, *b*, and R^2-values were similar to values reported in single-species allometric scaling studies. For example, de Simone and colleagues reported a scaling exponent, *b*, of 0.71 for CO vs. body mass (R^2 = 0.24), 1.83 for CO vs. height (R^2 = 0.19), and 1.15 for CO vs. BSA (R^2 = 0.25) in normotensive adults.[6] While CO and mean SC flow are not the same—CO is the measure of the total output of the heart—our scaling exponents, b, and R^2-values were similar: We found b values of 0.839 for mean SC flow vs. body mass (R^2 = 0.22), 2.34 for mean SC flow vs. height (R^2 = 0.26), and 1.56 for mean SC flow vs. BSA (R^2 = 0.29). Thus, our results followed a trend similar to de Simone's; mean flow vs. height had the greatest scaling exponent, and mean flow vs. body mass had the smallest scaling exponent. In addition, in both studies, mean flow vs. BSA had the highest R^2-value out of body mass, height, and BSA (de Simone did not compute FFBM).

Theoretical and experimental multispecies allometric scaling studies posit slightly lower scaling exponents for CO vs. body mass than those reported here. Theoretical studies predicted a scaling exponent, *b*, of 0.75 for CO as a function of body mass[9,28] while an experimental multispecies (mice to humans) analysis by Greve *et al*. found a scaling exponent of 0.69 (R^2 = 0.98) for CO as a function of body mass.[13] Multispecies allometric scaling studies enable much higher R^2-values than single species studies, as body masses between species may vary by more than an order of magnitude, and this greater variation "damps out" the comparatively smaller variations in CO vs. body mass within the same species.

R^2-values at the SC and IR Location

In general, our R^2-values were higher at the SC location compared to the IR location, indicating that body size was more predictive of mean flow at the SC location compared to the IR location. This could result from the fact that the same velocity encoding gradient was used for both the SC and IR locations. Because the IR aorta has lower volumetric flow and likely lower velocities, the potential for measurement error is higher, as has been

demonstrated experimentally.[8] The higher predictive accuracy of flow at the SC aorta may also be explained by differences among subjects in blood flow distribution to the mesenteric system. Flow at the SC level primarily supplies the kidneys, mesenteric and digestive organs, and lower limbs, and would be expected to have been relatively consistent among our subjects, in whom all limbs and organs were present. However, IR flow is delivered primarily to the inferior mesenteric artery (IMA) and lower limbs. IMA flow is extremely variable; in some patients, the IMA was totally occluded (patients 6, 7, 8, 13, 14, and 24 in Fig. 1), whereas in others it was greatly enlarged. For example, in patient 35, the splenic, hepatic, and renal arteries were relatively small and stenosed. As a result, this patient's IMA had adaptively enlarged to serve as a collateral circulation to the colon. Because the mesenteric and renal vessels likely took little flow and the IMA took much more flow, IR flow was much higher compared to other subjects. Indeed, this particular patient displayed the highest IR/SC flow ratio (0.57) within the cohort. Such variations in IR flow values resulted in poorer predictive accuracy (lower R^2-values) at the IR level. This is again in agreement with findings from Cheng *et al*., who also reported better correlation for their SC data than their IR data,[4] after using linear regression to assess the correlations between resting mean SC and IR flows vs. weight and height in young men and women. While all the correlations were weak (r = 0.00–0.402), Cheng *et al*. found that they were stronger at the SC aorta (r = 0.318 for mean SC flow vs. weight, r = 0.402 for mean SC flow vs. height) than at the IR level (r = 0.000 for mean IR flow vs. weight, r = 0.274 for mean IR flow vs. height). It is important to note, however, that their analysis was limited to 11 subjects and that linear regression was applied directly to a plots of mean flows vs. weight and mean flows vs. height, and not to the log–log plots of mean flows vs. weight and mean flows vs. height.

BSA Is Most Predictive of SC and IR Flow

In this study, the scaling exponent, b, calculated using linear regression was statistically significant for mean SC and IR flows vs. all metrics of body size with the exception of mean IR flow vs. height. This is not surprising, as body size seemed to be less predictive of mean IR flow (compared to mean SC flow) and since height is not necessarily predictive of body mass and thus blood flow demand. Mean SC and IR flows vs. BSA had the highest predictive accuracy (highest combined R^2-value), suggesting that when height and weight are available for a patient, the best way to predict mean SC and IR flows is from BSA. The peak-aligned and averaged SC and IR waveforms presented here can then be scaled such that average flow over a cardiac cycle equals the predicted flow for a given patient. The scale factor is simply the ratio of predicted flow to flow measured from the model cohort. Thus, if a person's predicted SC flow is 60.0 mL/s based on his or her BSA, the scale factor would be 60.0/51.2 = 1.17. Thus, the SC flow at each time-frame presented in Fig. 4 can be multiplied by 1.17 to generate a more accurate, patient-specific flow waveform. The allometric scaling equations for mean SC and IR flows vs. body mass and height may be useful when only body mass or height are available. Predicting flow from FFBM is ideal if only mean SC flow is desired, as mean SC flow vs. FFBM had the highest R^2-value (0.30), but had a comparatively low R^2-value for mean IR flow vs. FFBM (0.13).

Model Validation

For our model validation, the mean percent difference in predicted vs. measured flow was relatively low (−5.10 ± 18.9% for SC and −4.47 ± 25.3% for IR), suggesting that including patients 37 through 43 in the allometric scaling equations would likely change the equations little. The absolute value of the percent difference between predicted and measured flow for these patients was greater for IR flow than for SC flow (15.2% ± 10.9% for SC vs. 18.0% ± 16.9% for IR). This is not surprising given that the R^2-value for mean flow vs. BSA was lower for IR than for SC. Indeed, the low R^2-values found in our allometric scaling

equations suggest that our model may not predict individual mean flows or flow waveforms very well. However, despite this limitation, we propose that body size is the best predictor of mean flow, and we consider scaling by BSA (or any metric of body size) to be preferable to using a waveform from a single, young, healthy person, which would likely result in prescription of a waveform that may not only have an inaccurate mean flow, but might be triphasic, rather than biphasic in shape. The fact that our model was able to predict waveform shape quite well (when averaged over several patients) is encouraging (Fig. 6).

Limitations

The PC-MRI plane was prescribed perpendicular to the aorta according to the MRA and an oblique localizer scan to ensure that the image plane was completely orthogonal to the aorta. However, it is always possible that the resulting plane was not perfectly perpendicular to the aorta. In this case, however, the $\cos(\theta)$ factor by which the velocities for a tilted plane are *underestimated* is, in theory, equal to the factor by which the area of the vessel would be *overestimated*. Thus, the average flow, which is the product of the area and the average velocity, should be independent of the plane angle.[16] Second, although the PC-MRI sequence used respiratory compensation, breathing motion could also have caused artifacts and inaccuracy in measurement. In addition, eddy currents can induce significant gradient inhomogeneities that could lead to inaccurate flow computations. However, we have attempted to account for these inhomogeneities by using linear baseline correction. Lastly, it is important to note that half of the individual SC waveforms exhibited generally minimal reverse flow (while all of the individual IR waveforms exhibited significant reverse flow). However, because the averaged SC waveform does not display reverse flow, scaled versions of the averaged waveform will never exhibit reverse flow. Further investigations into why some patients exhibit reverse flow at the SC levels and others do not may be warranted. Additional future work includes imaging additional patients, incorporating other measures of body composition, and comparing flow waveforms to age-matched nonaneurysmal controls. In addition, scanning additional women with small AAAs may further elucidate features in AAA hemodynamics which contribute to the known differences in AAA pathophysiology in women, in whom aneurysmal disease is less common.

Another limitation lies in the fact that we assume that researchers will build and use models that begin at the SC level. These models require researchers to assume flow splits to the celiac, SMA, and renal arteries. However, getting these flow splits exactly correct is not essential. First, new boundary condition tuning methods can be used to match desired IR volumetric flow waveforms with a high level of fidelity without constraining the velocities at the IR location. Second, the uncertainty of celiac, SMA, and renal artery flow split is outweighed by the benefit of allowing IR flow to be aperiodic and asymmetric, especially when studying flow patterns and turbulence in AAAs that may originate just below the renal ostia.

The most important limitation of this study lies in the relatively low R^2-values. Although our R^2-values are comparable with other studies examining allometric scaling and flow, body size can only explain some of the difference between mean flows in patients. We found only weak or very weak correlations between mean flow and heart rate (SC: $R^2 = 0.019$, IR: $R^2 = 0.014$), age (SC: $R^2 = 0.049$, IR: $R^2 = 0.00089$), systolic blood pressure (SC: $R^2 = 0.083$, IR: $R^2 = 0.11$), diastolic blood pressure (SC: $R^2 = 0.10$, IR: $R^2 = 0.066$), and pressure pulse (SC: $R^2 = 0.010$, IR: $R^2 = 0.039$). Thus, although our results cannot predict individual waveforms perfectly, our data and methods are an important first step in estimating more accurate SC and IR boundary conditions for AAA simulation, and are preferable to using a waveform from a single, young healthy person.

Accuracy of PC-MRI Measurements

Several studies have examined the accuracy of PC-MRI measurements. Ku *et al*. found a maximum difference of 6% in volumetric flow measured by PC-MRI vs. flow predicted by computational simulations, [17] whereas Papaharilaou *et al*. found a spatially and temporally averaged root-mean-square-error of between 7.8% and 11.5% when comparing flow measured with PC-MRI and simulated flow.[24] In an elegant study, Evans *et al*. compared the volumetric flow measured in the ascending aorta and the main pulmonary artery in 10 patients—which should, in theory, be equal—and found an average difference of 5%.[8] Evans *et al*. also measured mean pulsatile flow using PC-MRI and plotted these measurements against known mean pulsatile flows from an *in vitro* model over a range of mean flows, with excellent agreement ($R^2 = 0.99$, $p = 0.0001$).[8] While not perfect, we feel that PC-MRI provides a sufficiently accurate, noninvasive method to measure blood flow.

In conclusion, we have assembled the largest existing compilation of aortic PC-MRI flow measurements in AAA patients to date. We have found that our peak-aligned, averaged waveforms exhibited a biphasic shape rather than the triphasic shape frequently seen in younger patients, and that BSA is most predictive of mean SC and IR flow. Thus, in the absence of specific flow information, mean SC and IR flows can be predicted from a particular patient's BSA, and the peak-aligned and averaged SC and IR waveforms presented here can be scaled such the mean flow over the cardiac cycle equals the patient's predicted mean flow. We hope that the results presented here will enable researchers to compute and use more accurate, patient-specific flow waveforms for *in vitro* and *in silico* simulation, as well as provide insight into the volumetric flow conditions proximal to the aneurysmal abdominal aorta. This may, in turn, lead to deeper insight into AAA growth and improve the design of aortic stent grafts used to treat AAAs.

Acknowledgments

The authors would like to thank Julie White and Mary McElrath for their assistance with patient recruitment, and Sandra Rodriguez and Anne Sawyer for their assistance with imaging. This work was supported by the National Institutes of Health (P50 HL083800 and P41 RR09784).

References

1. Bax L, Bakker CJ, Klein WM, Blanken N, Beutler JJ, Mali WP. Renal blood flow measurements with use of phase-contrast magnetic resonance imaging: normal values and reproducibility. J Vasc Interv Radiol. 2005; 16:807–814. [PubMed: 15947044]
2. Bosma RJ, van der Heide JJH, Oosterop EJ, de Jong PE, Navis G. Body mass index is associated with altered renal hemodynamics in non-obese healthy subjects. Kidney Int. 2004; 65:259–265. [PubMed: 14675058]
3. Cheng CP, Herfkens RJ, Taylor CA. Abdominal aortic hemodynamic conditions in healthy subjects aged 50–70 at rest and during lower limb exercise: *in vivo* quantification using MRI. Atherosclerosis. 2003; 168:323–331. [PubMed: 12801616]
4. Cheng CP, Herfkens RJ, Taylor CA. Comparison of abdominal aortic hemodynamics between men and women at rest and during lower limb exercise. J Vasc Surg. 2003; 37:118–123. [PubMed: 12514587]
5. Dalman RL, Tedesco MM, Myers J, Taylor CA. AAA disease: mechanism, stratification, and treatment. Ann NY Acad Sci. 2006; 1085:92–109. [PubMed: 17182926]
6. de Simone G, Devereux RB, Daniels SR, Mureddu G, Roman MJ, Kimball TR, Greco R, Witt S, Contaldo F. Stroke volume and cardiac output in normotensive children and adults. Assessment of relations with body size and impact of overweight. Circulation. 1997; 95:1837–1843. [PubMed: 9107171]
7. Draney MT, Zarins CK, Taylor CA. Three-dimensional analysis of renal artery bending motion during respiration. J Endovasc Ther. 2005; 12:380–386. [PubMed: 15943515]

8. Evans AJ, Iwai F, Grist TA, Sostman HD, Hedlund LW, Spritzer CE, Negrovilar R, Beam CA, Pelc NJ. Magnetic resonance imaging of blood-flow with a phase subtraction technique—*in vitro* and *in vivo* validation. Invest Radiol. 1993; 28:109–115. [PubMed: 8444566]
9. Feldman HA, McMahon TA. The 3/4 mass exponent for energy metabolism is not a statistical artifact. Respir Physiol. 1983; 52:149–163. [PubMed: 6878906]
10. Figueroa CA, Taylor CA, Yeh V, Chiou AJ, Zarins CK. Effect of curvature on displacement forces acting on aortic endografts: a 3-dimensional computational analysis. J Endovasc Ther. 2009; 16:284–294. [PubMed: 19642787]
11. Fraser KH, Meagher S, Blake JR, Easson WJ, Hoskins PR. Characterization of an abdominal aortic velocity waveform in patients with abdominal aortic aneurysm. Ultrasound Med Biol. 2008; 34:73–80. [PubMed: 17689855]
12. Garrow JS, Webster J. Quetelet index (w/h^2) as a measure of fatness. Int J Obes. 1985; 9:147–153. [PubMed: 4030199]
13. Greve JM, Les AS, Tang BT, Draney Blomme MT, Wilson NM, Dalman RL, Pelc NJ, Taylor CA. Allometric scaling of wall shear stress from mice to humans: quantification using cine phase-contrast MRI and computational fluid dynamics. Am J Physiol Heart Circ Physiol. 2006; 291:H1700–H1708. [PubMed: 16714362]
14. Holenstein R, Ku DN. Reverse flow in the major infrarenal vessels—a capacitive phenomenon. Biorheology. 1988; 25:835–842. [PubMed: 3076804]
15. Kim B, Soble JS, Stamos TD, Neumann A, Roberge J. Automated volumetric flow quantification using angle-corrected color Doppler image. Echocardiography. 2004; 21:399–408. [PubMed: 15209718]
16. Ku, JP. Numerical and Experimental Investigations of Blood Flow with Application to Vascular Bypass Surgeries. Stanford: Stanford University; 2003.
17. Ku JP, Elkins CJ, Taylor CA. Comparison of CFD and MRI flow and velocities in an *in vitro* large artery bypass graft model. Ann Biomed Eng. 2005; 33:257–269. [PubMed: 15868717]
18. Lederle FA, Johnson GR, Wilson SE, Chute EP, Littooy FN, Bandyk D, Krupski WC, Barone GW, Acher CW, Ballard DJ. Prevalence and associations of abdominal aortic aneurysm detected through screening. Ann Intern Med. 1997; 126:441–449. [PubMed: 9072929]
19. Les AS, Shadden SC, Figueroa CA, Park JM, Tedesco MM, Herfkens RJ, Dalman RL, Taylor CA. Quantification of hemodynamics in abdominal aortic aneurysms during rest and exercise using magnetic resonance imaging and computational fluid dynamics. Ann Biomed Eng. 2010 accepted.
20. Mills CJ I, Gabe T, Gault JH, Mason DT, Ross J, Braunwal E, Shilling JP. Pressure–flow relationships and vascular impedance in man. Cardiovasc Res. 1970; 4:405–417. [PubMed: 5533085]
21. Mosteller RD. Simplified calculation of body-surface area. N Engl J Med. 1987; 317:1098–1098. [PubMed: 3657876]
22. Olufsen MS, Peskin CS, Kim WY, Pedersen EM, Nadim A, Larsen J. Numerical simulation and experimental validation of blood flow in arteries with structured-tree outflow conditions. Ann Biomed Eng. 2000; 28:1281–1299. [PubMed: 11212947]
23. Osada T, Murase N, Kime R, Shiroishi K, Shimomura K, Nagata H, Katsumura T. Arterial blood flow of all abdominal-pelvic organs using doppler ultrasound: range, variability and physiological impact. Physiol Meas. 2007; 28:1303–1316. [PubMed: 17906396]
24. Papaharilaou Y, Doorly DJ, Sherwin SJ. Assessing the accuracy of two-dimensional phase-contrast MRI measurements of complex unsteady flows. J Magn Reson Imaging. 2001; 14:714–723. [PubMed: 11747028]
25. Schmidt-Nielsen, K. Scaling: Why Is Animal Size So Important?. Cambridge: Cambridge University Press; 1984.
26. Tang BT, Cheng CP, Draney MT, Wilson NM, Tsao PS, Herfkens RJ, Taylor CA. Abdominal aortic hemodynamics in young healthy adults at rest and during lower limb exercise: quantification using image-based computer modeling. Am J Physiol Heart Circ Physiol. 2006; 291:H668–H676. [PubMed: 16603687]
27. van der Molen AJ. Nephrogenic systemic fibrosis and the role of gadolinium contrast media. J Med Imaging Radiot Oncol. 2008; 52:339–350.

28. West GB, Brown JH, Enquist BJ. A general model for the origin of allometric scaling laws in biology. Science. 1997; 276:122–126. [PubMed: 9082983]

29. Womersley JR. Method for the calculation of velocity, rate of flow and viscous drag in arteries when the pressure gradient is known. J Physiol. 1955; 127:553–563. [PubMed: 14368548]

FIGURE 1.
The maximum intensity projections (MIPs) of the magnetic resonance angiography (MRA) scans for the model cohort (patients 1 through 36) are shown above.

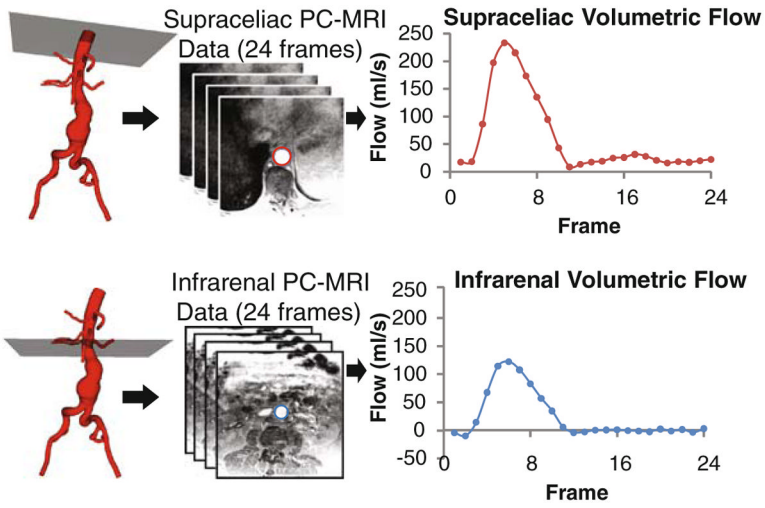

FIGURE 2.

The PC-MRI data are acquired at the supraceliac (SC) and infrarenal (IR) level in each patient. For each patient at each location, the velocities at each of 24 time frames are averaged over the luminal area and then multiplied by the luminal area to generate a flow value. After linear baseline correction, these flows are then assembled into volumetric flow waveforms. The example shown above is patient 3.

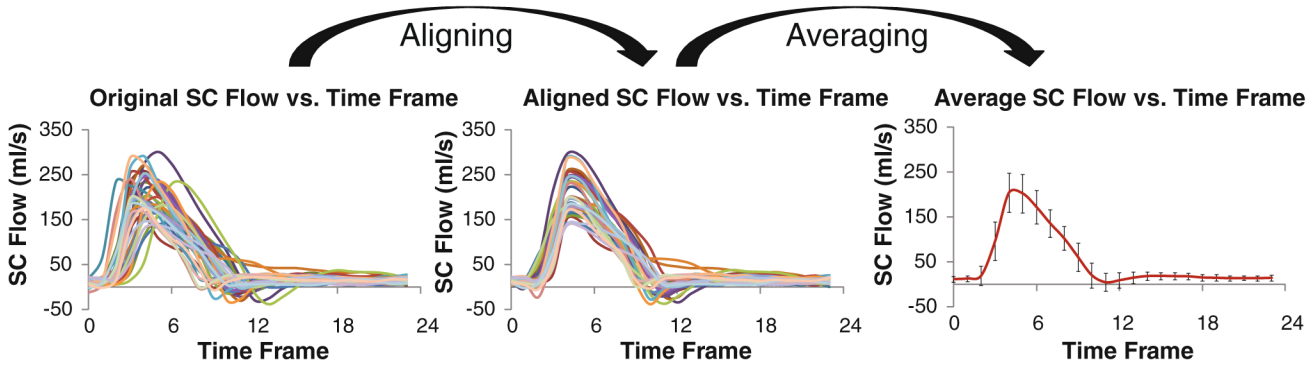

FIGURE 3.

The original waveforms (*left graph*) are interpolated to a 12-mode Fourier curves defined at 1000 points, peak-aligned (*middle graph*), and then down-sampled back to 24 time-frames and then averaged (*right graph*).

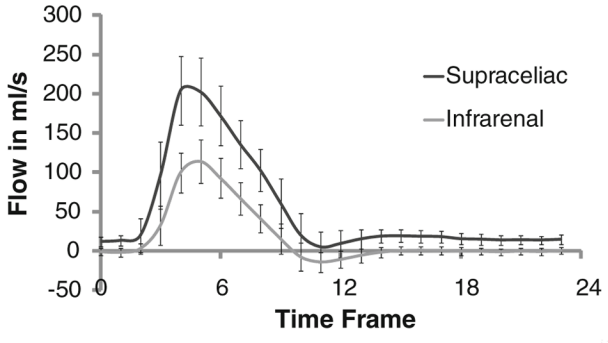

Frame	SC Flow (ml/s)	IR Flow (ml/s)
0	11.8	-1.08
1	13.1	-1.80
2	19.5	2.88
3	96.1	32.4
4	204	99.6
5	203	114
6	172	92.8
7	136	66.7
8	103	41.1
9	60.9	15.4
10	20.2	-7.55
11	4.75	-14.2
12	9.19	-10.9
13	15.0	-5.71
14	18.6	-1.67
15	18.9	0.333
16	18.4	0.702
17	18.0	0.594
18	15.3	-0.497
19	14.7	-0.481
20	13.7	-1.17
21	14.0	-0.306
22	13.7	-0.951
23	14.6	0.418

FIGURE 4.
The peak-aligned and averaged SC and IR flow waveforms and values are shown above. The waveforms were computed from the model cohort (patients 1 through 36).

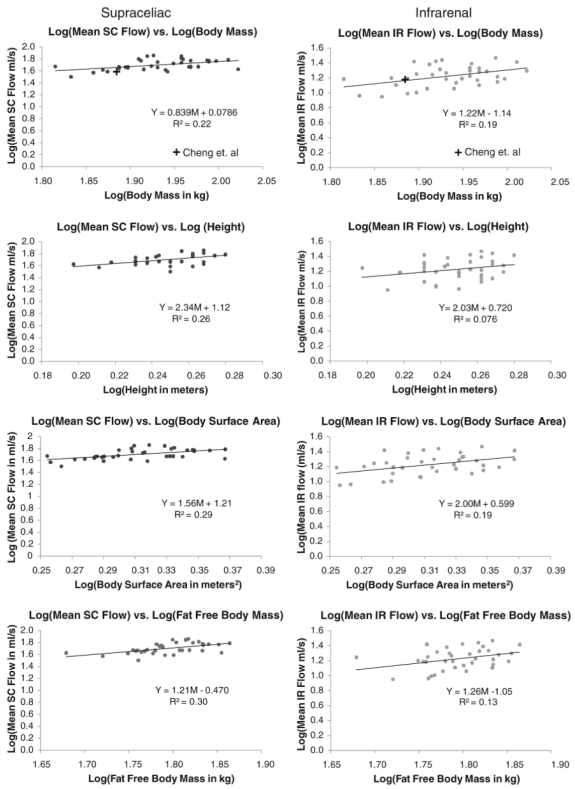

FIGURE 5.

The mean SC and IR flows vs. body mass, height, BSA, and fat-free body mass for the model cohort are shown above on log–log plots. Mean SC and IR flow measurements from Cheng *et al*. are plotted on the mean SC and IR flows vs. body mass plots.[3]

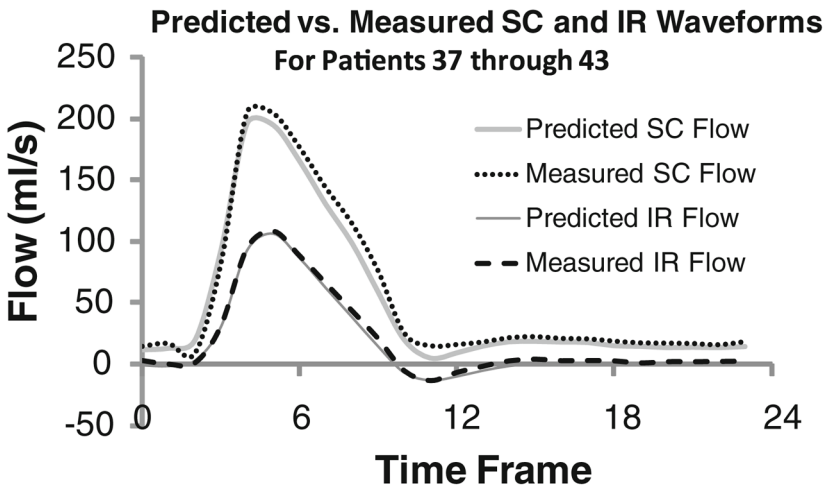

FIGURE 6.

The last seven AAA patients (the validation cohort, patients 37 though 43) were used to validate the model derived from the first 36 AAA patients (the model cohort). For the validation cohort, the mean SC and IR flows were predicted based on each patient's BSA. These predicted mean flows were used to scale the peak-aligned and averaged SC and IR waveforms presented in Fig. 4, thus generating predicted SC and IR waveforms. The predicted (averaged over seven patients) and measured (peak-aligned and averaged over seven patients) SC and IR waveforms are compared.

TABLE 1

Physiological parameters measured or calculated for the model (n = 36) and validation (n = 7) cohorts.

Variable	Model cohort (n = 36) Mean ± SD	Validation cohort (n = 7) Mean ± SD	Statistical significance
Male	35	7	
Female	1	0	
Age (years)	70.9 ± 6.73	70.0 ± 6.51	–
Average SC flow over cardiac cycle (mL/s)	51.2 ± 10.3	54.5 ± 11.3	–
Average IR flow over cardiac cycle (mL/s)	17.5 ± 5.44	18.9 ± 9.11	–
IR flow/SC flow ratio	0.343 ± 0.0843	0.338 ± 0.0971	–
Heart rate at SC acquisition (bpm)	63.3 ± 11.0	59.6 ± 9.13	–
Heart rate at IR acquisition (bpm)	62.9 ± 10.5	59.6 ± 9.14	–
Weight (kg)	86.2 ± 9.53	84.9 ± 12.6	–
Height (m)	1.77 ± 0.0760	1.74 ± 0.0620	–
Body surface area (m^2)	2.06 ± 0.0143	2.02 ± 0.169	–
Fat-free body mass (kg)	62.5 ± 5.56	60.8 ± 5.39	–
Body mass index (kg/m^2)	27.4 ± 2.74	28.1 ± 3.47	–
Systolic blood pressure (mmHg)	143 ± 15.9	140 ± 17.4	–
Diastolic blood pressure (mmHg)	84.4 ± 9.92	87.6 ± 4.76	–
eGFR (mL/min/1.73 m^2)	78.1 ± 18.2	88.4 ± 25.0	–

Values are mean ± standard deviation (SD). The patients' gender distribution, age, mean SC and IR flow, heart rate, four metrics of body size and blood pressures were measured or calculated. eGFR indicates estimated glomerular filtration rate and is a necessary measure of kidney function prior to gadolinium usage. A dash (–) for statistical significance indicates that the model and validation cohort were not statistically different (p>0.05) for the given parameter.

TABLE 2

Allometric scaling equations for mean supraceliac and infrarenal flows vs. body mass, height, body surface area, and fat-free body mass.

Equation	R^2	*p* Value for *b*	*p* Value for log(Y_0)
Supraceliac			
$\mathrm{SC\,flow_{mean}} = 1.20\,(\mathrm{body\ mass})^{0.839}$	0.22	$p<0.005$	–
$\mathrm{SC\,flow_{mean}} = 13.1\,(\mathrm{height})^{2.34}$	0.26	$p<0.005$	$p \ll 0.001$
$\mathrm{SC\,flow_{mean}} = 16.4\,(\mathrm{body\ surface\ area})^{1.56}$	0.29	$p<0.001$	$p \ll 0.001$
$\mathrm{SC\,flow_{mean}} = 0.339\,(\mathrm{fat\ free\ body\ mass})^{1.21}$	0.30	$p<0.001$	–
Infrarenal			
$\mathrm{IR\,flow_{mean}} = 0.0732\,(\mathrm{body\ mass})^{1.22}$	0.19	$p<0.01$	–
$\mathrm{IR\,flow_{mean}} = 5.24\,(\mathrm{height})^{2.03}$	0.076	–	$p<0.05$
$\mathrm{IR\,flow_{mean}} = 3.98\,(\mathrm{body\ surface\ area})^{2.00}$	0.19	$p<0.01$	$p<0.05$
$\mathrm{IR\,flow_{mean}} = 0.0900\,(\mathrm{fat\ free\ body\ mass})^{1.26}$	0.13	$p<0.05$	–

The allometric scaling equations for the mean SC and IR flows (mL/s) vs. body mass (kg), height (m), body surface area (m^2), and fat free body mass (kg) are presented above. The R^2 values from the linear regression of the log–log plots are presented, as well as the *p*-values for the scaling exponent, *b*, and for the log(Y_0). A dash (−) for *p*-value indicates that the value was not statistically significant ($p>0.05$).

TABLE 3

A comparison between measured and predicted mean SC and IR flows for the seven patients in the validation cohort.

	Body size metrics			SC flow				IR flow			
	Height (m)	Body mass (kg)	BSA (m^2)	Predicted SC flow (mL/s)	Measured SC flow (mL/s)	% Diff. SC flow	Abs (% Diff. SC flow)	Predicted IR flow (mL/s)	Measured IR flow (mL/s)	% Diff. IR flow	Abs (% Diff. IR flow)
Patient 37	1.78	71.7	1.88	44.0	43.0	2.27	2.27	14.1	11.2	26.1	26.1
Patient 38	1.83	107	2.33	61.2	72.9	−16.0	16.0	21.6	38.5	−44.0	44.0
Patient 39	1.68	86.6	2.01	56.3	45.2	24.6	24.6	16.1	16.7	−4.07	4.07
Patient 40	1.78	96.2	2.18	55.3	50.9	8.58	8.58	18.9	15.7	20.6	20.6
Patient 41	1.68	78.0	1.91	44.9	46.1	−2.66	2.66	14.5	14.4	0.326	0.326
Patient 42	1.68	80.7	1.94	46.1	64.6	−28.6	28.6	15.0	14.9	0.387	0.387
Patient 43	1.75	74.4	1.90	44.7	58.8	−23.9	23.9	14.4	20.8	−30.6	30.6
Mean	**1.74**	**84.9**	**2.02**	**50.3**	**54.5**	**−5.10**	**15.2**	**16.3**	**18.9**	**−4.47**	**18.0**
SD	**0.0620**	**12.6**	**0.169**	**7.06**	**11.3**	**18.9**	**10.9**	**2.83**	**9.11**	**25.3**	**16.9**

Height and body mass were measured at study intake. Predicted mean SC and IR flows were calculated from each patient's body surface area (BSA) based on the allometric scaling equations derived from the model cohort. SD is standard deviation and % Diff. is the percent difference between predicted and measured flows. Abs (% Diff.) indicates the absolute value of the percent difference between predicted and measured flows.